

Article

Optimal Selection among Various Three-Phase Four-Wire Back-to-Back (BTB) Converters with Comparative Analysis for Wave Energy Converters

Chan Roh 

Division of Marine System Engineering, Korea Maritime and Ocean University, 727 Taejong-ro, Yeongdo-gu, Busan 49112, Republic of Korea; rohchan@kmou.ac.kr

Abstract: Wave energy converters are attracting attention as an energy source that can respond to climate change. In order to increase the energy efficiency of the wave energy converters, efficient power converters are also required. The efficient converters require operation at a low switching frequency, which increases the weight and volume of the passive components. Therefore, in this paper, the performance of various types of topologies is compared to select the optimal power converter for wave energy converters. In order to cope with the unbalanced operation and unbalanced load of renewable energy, in this paper, the topology of the four-leg type is analyzed centrally. In addition, the analysis was performed by applying the model predictive control that can quickly respond to the rapid energy change of wave energy. In addition, model predictive control was applied to the four-leg converter analyzed in this paper because it is suitable for application to atypical topologies. For performance analysis of various types of topology, the loss and efficiency of each converter were analyzed by applying a loss analysis model, and output current harmonics and leakage current characteristics, capacitor voltage fluctuation rate, etc., were additionally analyzed at various switching frequencies. In conclusion, the three-level four-leg converter showed up to 2.28% and 2.7% higher efficiency under balanced and unbalanced operating conditions.

Keywords: multilevel topology; three-phase four-leg topology; model predictive control; symmetric operation; asymmetric operation; power losses; efficiency



Citation: Roh, C. Optimal Selection among Various Three-Phase Four-Wire Back-to-Back (BTB) Converters with Comparative Analysis for Wave Energy Converters. *Processes* **2023**, *11*, 1463. <https://doi.org/10.3390/pr11051463>

Academic Editors: George J. Tsekouras and Fotios D. Kanellos

Received: 31 March 2023
Revised: 3 May 2023
Accepted: 9 May 2023
Published: 11 May 2023



Copyright: © 2023 by the author. Licensee MDPI, Basel, Switzerland. This article is an open access article distributed under the terms and conditions of the Creative Commons Attribution (CC BY) license (<https://creativecommons.org/licenses/by/4.0/>).

1. Introduction

Excessive use of fossil fuel power plants has produced abundant greenhouse gases, a major cause of climate change. Renewable energy can partially replace fossil-fueled power plants and has been proposed as an alternative to address climate change. For this reason, wave energy has been attracting attention in the past 20 years to alleviate the energy demand problem, and the development of wave energy systems has been carried out [1]. The global theoretical wave energy potential is estimated at 16,000 TWh per year [2,3], which could make a significant contribution to meeting the growing global energy demand. In particular, the temporal characteristics of wave energy can compensate for the discontinuity of other renewable energy sources, such as wind power and solar power [4–6].

An important goal of renewable energy is to lower the cost of electricity generation through increased energy efficiency. In other words, an efficient converter topology has been emphasized in terms of power converters due to increased energy costs and environmental concerns. One possible way to achieve higher converter efficiency is to operate at a lower switching frequency. However, wave energy converters need to reduce the volume and weight of passive components to reach high power densities due to space constraints. This requires high switching frequencies. However, a two-level converter based on IGBT (Insulated Gate Bipolar Transistor) causes excessive loss when the switching frequency is increased, but wave energy converters are still applied to most of them. Therefore, it is

difficult to meet both efficiency requirements and technical performance requirements with a two-level converter, and three-level converters for wave energy converters have been discussed [7–9]. Excellent efficiency at higher switching frequencies due to low switching losses despite the increased complexity and high initial cost makes the three-level topology attractive for wave power applications.

From a wave power system point of view, the benefits of using a three-level converter are not limited to the converter itself. The main parts of this modern three-phase AC-DC-AC converter system are shown in Figure 1. On the grid side, electromagnetic interference (EMI) input filters are usually required to attenuate current harmonics. From there, the three-level output voltage waveform reduces the boost inductance required and, consequently, the boost inductor volume and losses. Also, on the generator side, harmonic losses are significantly reduced when a three-level voltage waveform is applied. The positive impact is reduced mechanical insulation stress and reduced overvoltage due to long motor cables [10], which can be problematic in two-level converter applications [11].

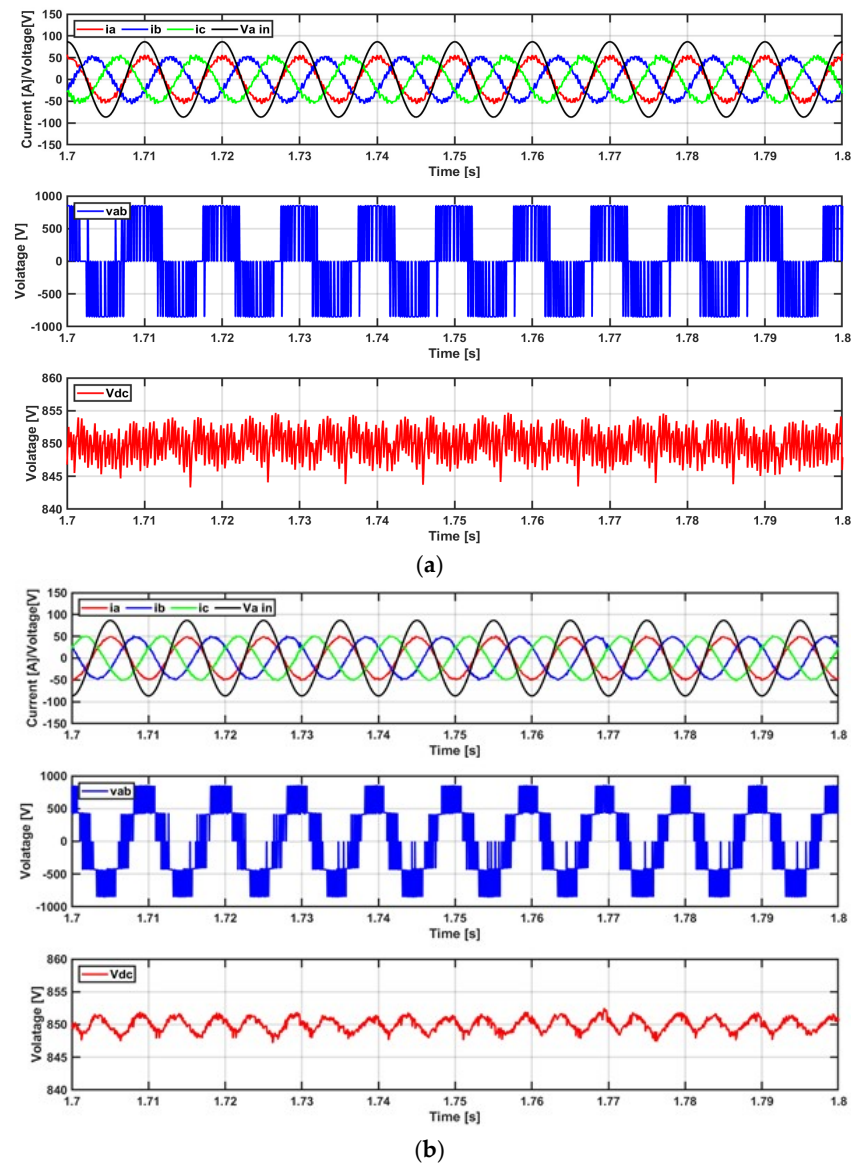


Figure 1. Comparison of performance of (a) two-level converter and (b) three-level converter with model predictive control.

In this paper, the competitiveness of the three-level topology for wave power applications is analyzed in terms of efficiency and performance. The paper characterizes topology loss and efficiency, topology output current harmonics and leakage current. Additionally, because of the nature of wave energy converter, it is necessary to supply power to an independent load, so the analysis is focused on the four-leg topology to respond to unbalanced loads. An unbalanced load is caused by unbalance of three-phase and single-phase loads in independent operation and can occur when nonlinear loads, such as factories and warehouses (for example, island microgrids), increase rapidly. The power range considered is limited to 5–30 kW, considering a single wave power operating area. Many fields already use various topologies of multilevel converters [12] and apply control methods [13], but in this study, an analysis was performed based on the topology applied to wave power devices so far. In [12], research on obtaining fast responses by applying artificial intelligence-based indirect space vector control was also conducted. Likewise, in [13], research on cascaded H-bridge converters for large-capacity converters was conducted, but it has not yet been applied to wave power devices.

Unlike the control methods for various topologies described above, the four-leg-based power converters focused on in this study have a special configuration, so they are not suitable for conventional linear controllers (PI controller-based pulse width modulation, PI-based PWM) or three-dimensional space vector pulse widths. Complexity increases in modulation (SVPWM) application [14–18]. Obviously, many studies have been conducted, and applicability is not impossible, but model-based current control is more advantageous for converters with special configurations because it can configure a simple and intuitive controller [19,20]. That is, even if complex control variables exist in an unusual topology, such as a four-wire converter, it may have the advantage of being easy to apply. Recently, many academic studies have been conducted on the application of model prediction to various topologies [21–23].

In conclusion, we analyze the four topologies that have been widely applied to the existing wave power generation. The four-leg topology of the two-level converter and three-level neutral clamp converter [24] is for comparison. More multilevel converters may be considered in the future [25,26]. In addition, each topology was analyzed for performance by applying model predictive control to reflect unusual behavioral characteristics. This model's predictive control is excellent in responding to rapidly changing wave energy due to its fast response. Performance for each topology compares efficiency and performance under varying conditions, including balanced load and unbalanced load conditions. In addition, the performance comparison according to the control sampling frequency affects the topology efficiency. These analyses can provide criteria for a topology suitable for wave power generation and provide guidelines for applicability.

2. Three-Phase Four-Leg Topology Configurations and Control Method

The power converter for wave energy converter consists of an AC/DC converter that converts the AC power of a generator into DC power and a DC/AC inverter that converts DC power into AC power. Along with the technological advancement of the wave energy converter, the power conversion system for wave energy converter also needs the application of a multilevel converter according to the increase in capacity. Among other renewable energy sources, wind turbines use two-level power converters for tens of kW to hundreds of kW generators, but multilevel converters are applied for generators of MW or higher. As a result, the increase in output power has made it inevitable to apply multilevel converters. Multilevel converters (three-level NPC type converters) are not only applied in various fields but also have various advantages, such as reducing harmonics according to the increase in output voltage level and reducing the size of passive filters, so they will be applied to wave power generators. Figure 1 compares the output characteristics of the two-level topology and the three-level topology under the wave power single module rating (30 kW) operating condition. The three-level topology exhibits excellent performance, such as low total harmonic distortion and low voltage stress under the same input conditions.

In other words, the three-level topology may have sufficiently excellent performance in wave energy converters.

General three-wire power converters have limitations in application depending on the operating conditions of the load. In other words, normal current control is not possible in an unbalanced load operation. These limitations can be protected by the operation of a four-wire power converter. In addition, the four-wire power converter has an excellent advantage in leakage current control in terms of safety. Since the wave energy converter needs independent operation and response to unbalanced loads, in this study, a characteristic analysis was performed using a four-leg topology. Figure 1 shows a three-level, four-leg topology for application in a wave power system with leakage capacitors.

In this paper, various four-leg topologies were compared and analyzed to select a suitable topology for application to wave energy converter. Comparison is performed from a two-level topology that has been widely applied in the past to a three-level topology to improve output performance. In this study, a total of four types of topologies were compared, and Figure 2 shows the configuration of the topology applied in this study. In order to apply the wave power characteristics, the analysis was focused on the AC/DC converter related to the input energy. DC/AC inverters have similar operating characteristics and are not described separately. The topology of the four-leg type is a rectifier with a two-level three-leg four-wire structure (Figure 3a), a three-phase two-level four-leg structure rectifier (Figure 3b), and a three-level three-leg four-wire structure. It consists of a rectifier (Figure 3c) and a rectifier with a three-level, four-leg structure (Figure 3d).

In this paper, a model predictive control that can have a fast response is applied to respond to wave energy. In addition, the model predictive control can provide the convenience of control due to the characteristics of the four-leg topology having nonlinear characteristics. Furthermore, in the case of a three-level topology, the model predictive control can have sufficient advantages because the control variable increases.

In order to apply the model predictive control to the converters shown in Figure 3, the relationship between the switching state and the output voltage according to each converter must be considered. That is, it is necessary to observe the change of the control variable according to the switching state of each converter. The control of the converter consists of two parts. It can be seen in Figure 4 that a part of the capacitor voltage control is added to the three-level converter rather than the two-level converter. This part increases the complexity of the control.

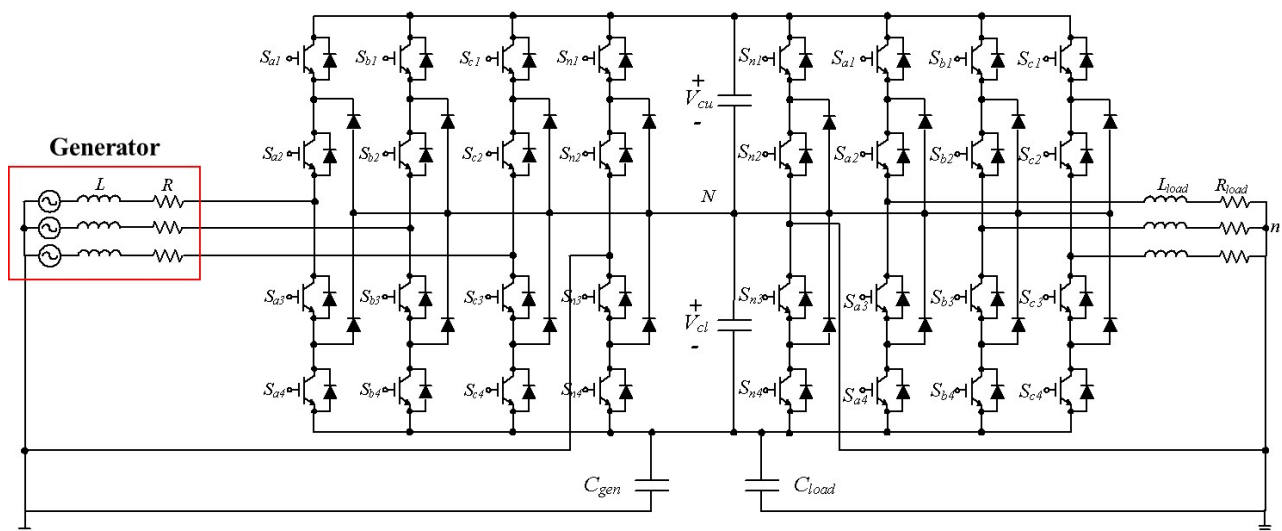


Figure 2. Circuit diagram of three-level four-leg back-to-back (BTB) converter with leakage capacitors.

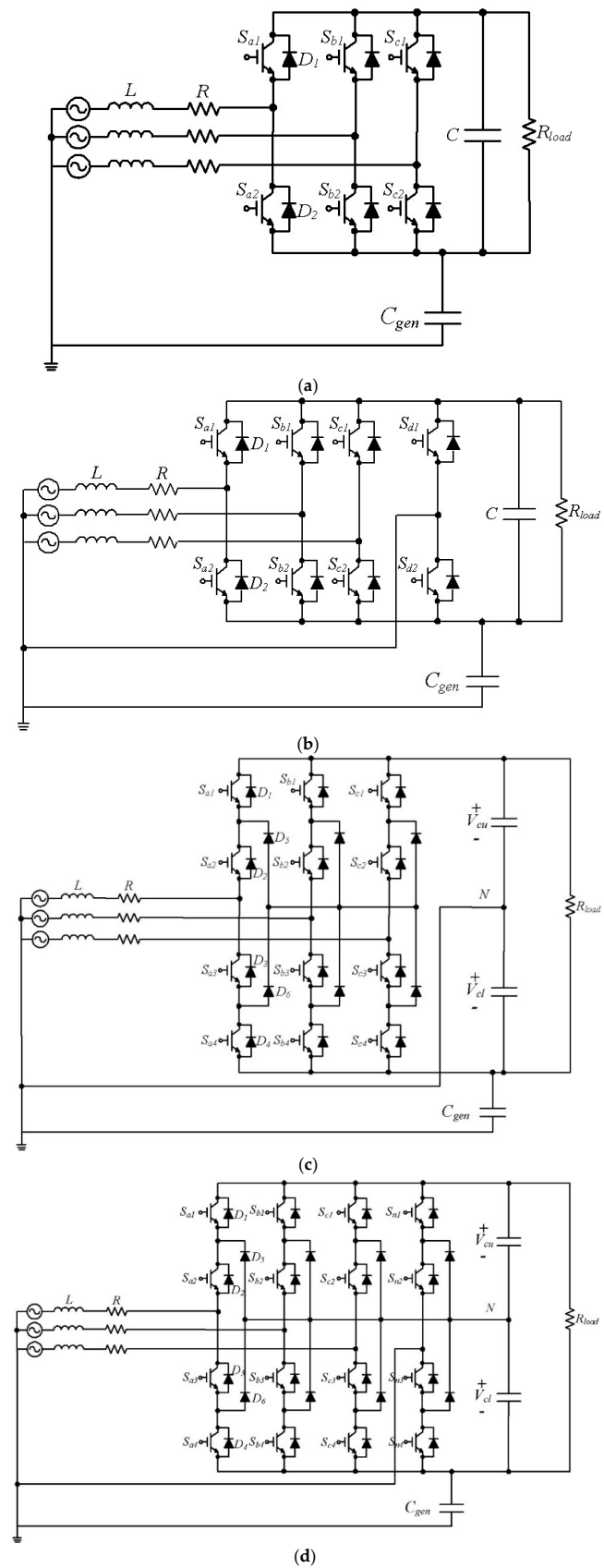


Figure 3. Three-phase four-wire AC/DC converter block diagram (a) two-level/three-leg four-wire topology (b) two-level/four-leg topology (c) three-level/three-leg four-wire topology (d) three-level/four-leg topology.

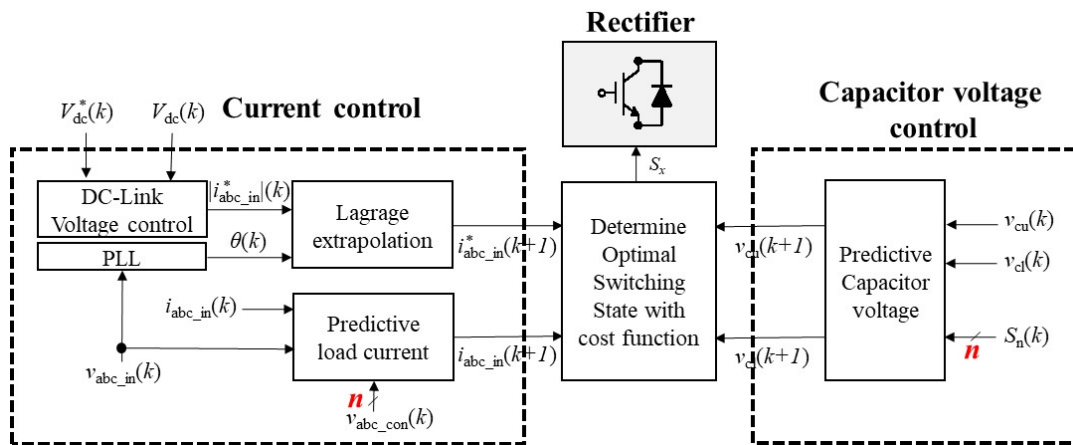


Figure 4. Block diagram of model predictive control for AC/DC four-leg converter.

The current control part of applying the model predictive control to the converter can be expressed as follows by using the R-L filter (R_f, L_f) and the input voltage (v_{abc_in}) and the input current (i_{abc_in}) for the input AC voltage of the converter.

$$\begin{bmatrix} v_{a_in} \\ v_{b_in} \\ v_{c_in} \end{bmatrix} = R_f \begin{bmatrix} i_{a_in} \\ i_{b_in} \\ i_{c_in} \end{bmatrix} + L_f \frac{d}{dt} \begin{bmatrix} i_{a_in} \\ i_{b_in} \\ i_{c_in} \end{bmatrix} + \begin{bmatrix} v_{a_con} \\ v_{b_con} \\ v_{c_con} \end{bmatrix} \quad (1)$$

Equation (1) can be expressed as follows if the next step current is predicted based on the discrete model.

$$\begin{bmatrix} i_{a_in}(k+1) \\ i_{b_in}(k+1) \\ i_{c_in}(k+1) \end{bmatrix} = \left(1 - L_f^{-1} T_{sp} R_f\right) \begin{bmatrix} i_{a_in}(k) \\ i_{b_in}(k) \\ i_{c_in}(k) \end{bmatrix} + L_f^{-1} T_{sp} \begin{bmatrix} v_{a_in}(k) - v_{a_con}(k) \\ v_{b_in}(k) - v_{b_con}(k) \\ v_{c_in}(k) - v_{c_con}(k) \end{bmatrix} \quad (2)$$

Based on Equation (2), the optimal switching state can be selected by predicting the load current of the next step using all voltage states that the converter can make and comparing it with the reference current. The magnitude of the reference current shown in Figure 4 is based on the difference between the reference DC-Link voltage and the current DC voltage, using a PI controller to configure the controller [27]. Then, the phase of the input current is extracted based on the PLL algorithm to control the power factor to one. The current reference generated in this way can obtain the predicted reference current based on Lagrange extrapolation [28].

The optimal switching state is selected through an optimization problem, and the optimization method is as follows.

$$G_{current} = |i_{abc_in}^*(k+1) - i_{abc_in}(k+1)| \quad (3)$$

Capacitor voltage control is essential for a three-level converter, and the variability of the capacitor voltage based on the current of the capacitor is expressed as:

$$\frac{d}{dt} \begin{bmatrix} V_{cu} \\ V_{cl} \end{bmatrix} = C_{dc}^{-1} \begin{bmatrix} i_{cu} \\ i_{cl} \end{bmatrix} \quad (4)$$

i_{cu}, i_{cl} denote currents flowing through the upper capacitor and the lower capacitor, and C_{dc}^{-1} denotes the capacitance of the capacitor, respectively. If this is expressed in discrete-model like current control, the next step capacitor voltage can be calculated as follows:

$$\begin{bmatrix} v_{cu}(k+1) \\ v_{cl}(k+1) \end{bmatrix} = \begin{bmatrix} v_{cu}(k) \\ v_{cl}(k) \end{bmatrix} + C_{dc}^{-1} T_{sp} \begin{bmatrix} i_{cu}(k) \\ i_{cl}(k) \end{bmatrix} \quad (5)$$

As a result, the optimization method of the three-level converter is as follows and consists of a part for current control and a part for capacitor voltage balancing control.

$$G_{total} = \left| i_{abc_in}^*(k+1) - i_{abc_in}(k+1) \right| + \lambda_{cap} |v_{cu}(k+1) - v_{cl}(k+1)| \quad (6)$$

In the case of the three-level converter, it can be superior to the conventional two-level converter in terms of output performance, but the number of voltage vectors to be considered for current control and capacitor voltage balancing control increases significantly [29]. The voltage vectors and switching states to be considered in the converters applied in this study are shown in Tables 1–4 below.

Table 1. Input voltage according to the switching state of the two-level three-leg.

Voltage Vectors	Switching State	Voltage			Voltage Vectors	Switching State	Voltage		
		v_a	v_b	v_c			v_a	v_b	v_c
v_1	PPP	1	1	1	v_5	NPP	0	1	1
v_2	NNN	0	0	0	v_6	PNN	1	0	0
v_3	NNP	0	0	1	v_7	PNP	1	0	1
v_4	NPN	0	1	0	v_8	PPN	1	1	0

Table 2. Input voltage according to the switching state of the two-level four-leg.

Voltage Vectors	Switching State	Voltage			Voltage Vectors	Switching State	Voltage		
		v_a	v_b	v_c			v_a	v_b	v_c
v_1	PPPP	0	0	0	v_9	PPPN	1	1	1
v_2	NNNP	−1	−1	−1	v_{10}	NNNN	0	0	0
v_3	PNNP	0	−1	−1	v_{11}	PNNN	1	0	0
v_4	PPNP	0	0	−1	v_{12}	PPNN	1	1	0
v_5	NPNP	−1	0	−1	v_{13}	NPNN	0	1	0
v_6	NPPP	−1	0	0	v_{14}	NPPN	0	1	1
v_7	NNPP	−1	−1	0	v_{15}	NNPN	0	0	1
v_8	PNPP	0	−1	0	v_{16}	PNPN	1	0	1

Table 3. Three-level three-leg input voltage state according to the switching state.

Voltage Vectors	Switching State	Voltage			Voltage Vectors	Switching State	Voltage		
		v_a	v_b	v_c			v_a	v_b	v_c
v_1	PPP	0.5	0.5	0.5	v_{15}	ONO	0	−0.5	0
v_2	NNN	−0.5	−0.5	−0.5	v_{16}	PON	0.5	0	−0.5
v_3	OOO	0	0	0	v_{17}	OPN	0	0.5	−0.5
v_4	POO	0.5	0	0	v_{18}	NPO	−0.5	0.5	0
v_5	ONN	0	−0.5	−0.5	v_{19}	NOP	−0.5	0	0.5
v_6	PPO	0.5	0.5	0	v_{20}	ONP	0	−0.5	0.5
v_7	OON	0	0	−0.5	v_{21}	PNO	0.5	−0.5	0
v_8	OPO	0	0.5	0	v_{22}	PNN	0.5	−0.5	−0.5
v_9	NON	−0.5	0	−0.5	v_{23}	PPN	0.5	0.5	−0.5
v_{10}	OPP	0	0.5	0.5	v_{24}	NPN	−0.5	0.5	−0.5
v_{11}	NOO	−0.5	0	0	v_{25}	NPP	−0.5	0.5	0.5
v_{12}	OOP	0	0	0.5	v_{26}	NNP	−0.5	−0.5	0.5
v_{13}	NNO	−0.5	−0.5	0	v_{27}	PNP	0.5	−0.5	0.5
v_{14}	POP	0.5	0	0.5					

Table 4. Input voltage according to the switching state of the three-level four-leg.

Voltage Vectors	Switching State	Voltage			Voltage Vectors	Switching State	Voltage		
		v_{an}	v_{bn}	v_{cn}			v_{an}	v_{bn}	v_{cn}
v_1	NNNN	0	0	0	v_{42}	OOP	-0.5	-0.5	-0.5
v_2	NNNO	-0.5	-0.5	-0.5	v_{43}	OOPN	0.5	0.5	1
v_3	NNNP	-1	-1	-1	v_{44}	OOP	0	0	0.5
v_4	NNON	0	0	0.5	v_{45}	OOPP	-0.5	-0.5	0
v_5	NNOO	-0.5	-0.5	0	v_{46}	OPNN	0.5	1	0
v_6	NNOP	-1	-1	-0.5	v_{47}	OPNO	0	0.5	-0.5
v_7	NNPN	0	0	1	v_{48}	OPNP	-0.5	0	-1
v_8	NNPO	-0.5	-0.5	0.5	v_{49}	OPON	0.5	1	0.5
v_9	NNPP	-1	-1	0	v_{50}	OPOO	0	0.5	0
v_{10}	NONN	0	0.5	0	v_{51}	OPOP	-0.5	0	-0.5
v_{11}	NONO	-0.5	0	-0.5	v_{52}	OPPN	0.5	1	1
v_{12}	NONP	-1	-0.5	-1	v_{53}	OPPO	0	0.5	0.5
v_{13}	NOON	0	0.5	0.5	v_{54}	OPPP	-0.5	0	0
v_{14}	NOOO	-0.5	0	0	v_{55}	PNNN	1	0	0
v_{15}	NOOP	-1	-0.5	-0.5	v_{56}	PNN	0.5	-0.5	-0.5
v_{16}	NOPN	0	0.5	1	v_{57}	PNNP	0	-1	-1
v_{17}	NOPO	-0.5	0	0.5	v_{58}	PNON	1	0	0.5
v_{18}	NOPP	-1	-0.5	0	v_{59}	PNOO	0.5	-0.5	0
v_{19}	NPNN	0	1	0	v_{60}	PNOP	0	-1	-0.5
v_{20}	NPNO	-0.5	0.5	-0.5	v_{61}	PNPN	1	0	1
v_{21}	NPNP	-1	0	-1	v_{62}	PNPO	0.5	-0.5	0.5
v_{22}	NPON	0	1	0.5	v_{63}	PNPP	0	-1	0
v_{23}	NPOO	-0.5	0.5	0	v_{64}	PONN	1	0.5	0
v_{24}	NPOP	-1	0	-0.5	v_{65}	PONO	0.5	0	-0.5
v_{25}	NPPN	0	1	1	v_{66}	PONP	0	-0.5	-1
v_{26}	NPPO	-0.5	0.5	0.5	v_{67}	POON	1	0.5	0.5
v_{27}	NPPP	-1	0	0	v_{68}	POOO	0.5	0	0
v_{28}	ONNN	0.5	0	0	v_{69}	POOP	0	-0.5	-0.5
v_{29}	ONNO	0	-0.5	-0.5	v_{70}	POP	1	0.5	1
v_{30}	ONNP	-0.5	-1	-1	v_{71}	POPO	0.5	0	0.5
v_{31}	ONON	0.5	0	0.5	v_{72}	POPP	0	-0.5	0
v_{32}	ONOO	0	-0.5	0	v_{73}	PPNN	1	1	0
v_{33}	ONOP	-0.5	-1	-0.5	v_{74}	PPNO	0.5	0.5	-0.5
v_{34}	ONPN	0.5	0	1	v_{75}	PPNP	0	0	-1
v_{35}	ONPO	0	-0.5	0.5	v_{76}	PPON	1	1	0.5
v_{36}	ONPP	-0.5	-1	0	v_{77}	PPOO	0.5	0.5	0
v_{37}	OONN	0.5	0.5	0	v_{78}	PPOP	0	0	-0.5
v_{38}	OONO	0	0	-0.5	v_{79}	PPPN	1	1	1
v_{39}	OONP	-0.5	-0.5	-1	v_{80}	PPPO	0.5	0.5	0.5
v_{40}	OON	0.5	0.5	0.5	v_{81}	PPPP	0	0	0
v_{41}	OOOO	0	0	0					

3. Four-Leg Topology Loss Analysis Model

Estimating the power dissipation allows us to estimate the efficiency of each converter, and this estimate can be used to evaluate various converter topologies before assembling and testing the converter. Therefore, the power loss estimation provides the designer with an optimization method. It can also accurately estimate semiconductor thermal stresses under various operating conditions to design appropriate protection strategies to prevent excessive thermal stresses.

A simple model that describes a semiconductor in terms of voltage source drop and resistance is useful for determining conduction losses but not suitable for estimating switching losses. As an alternative to simple and complex semiconductor models, simulations with ideal switches and diodes can be fast. With an ideal switch, there is a close match between the simulated current and voltage if the conduction voltage drop of the real device is insignificant. Therefore, a method was introduced to estimate the power dissipation in the simulation using an ideal switch and then introduce a post-process to reflect the actual semiconductor behavior. A flow chart of the power device loss calculation is shown in Figure 5.

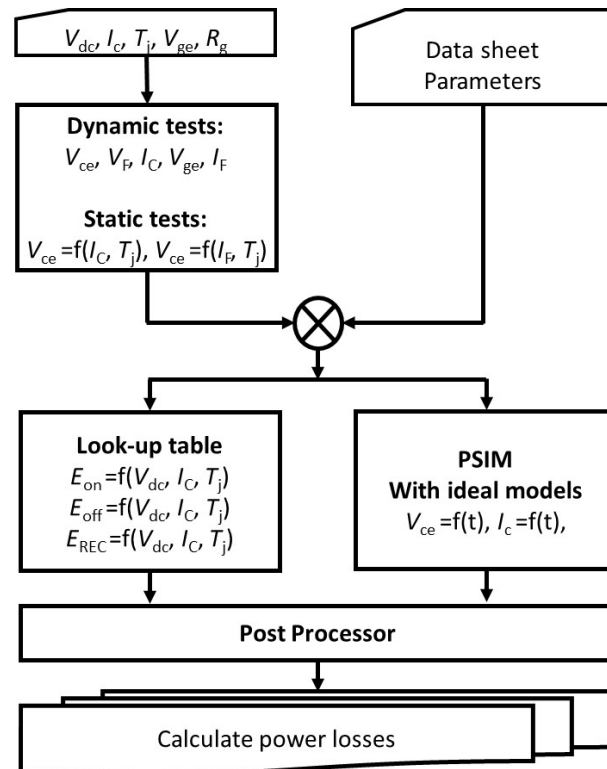


Figure 5. The flowchart of power device loss calculation for a three-phase four-wire DC/AC inverter.

High-speed simulation by PSIM, together with the ideal model of the power device, can be used to determine the voltage and current of the switching device at the moment of switching. A post-processor program using linear equations is run to calculate total device losses based on switching energy losses and on-state voltage losses over voltage, current, and junction temperature. SiC Mosfet turn-on energy loss (E_{ON}), turn-off energy loss (E_{OFF}), and diode reverse recovery loss based on the data sheet as a function of DC voltage (V_{DC}), collector current (I_C), junction temperature (T_j), and gate resistance (R_g) (E_{REC}) is calculated. Finally, SiC Mosfet power dissipation and diode power dissipation are calculated based on the switching frequency (f_{sw}) [30].

A post-processor program is used to calculate semiconductor losses after a quick simulation using ideal switches and diodes. Switching moments are detected using sharp edges in voltage and current waveforms. A positive voltage edge occurs at the moment of turning off, and a negative voltage at the moment of turning on. At each switching moment, the turn-on voltage value, turn-on current, turn-off voltage and turn-off current are sensed according to the positive or negative voltage edge. At that time, the post-processor uses linear functions derived from the datasheet to calculate the SiC Mosfet turn-on energy loss (E_{ON}), SiC Mosfet turn-off energy loss (E_{OFF}) and diode turn-off energy loss (E_{REC}). The

turn-on power (P_{ON}), turn-off power (P_{OFF}), and diode turn-off losses (P_{REC}) are calculated as follows:

$$P_{ON} = \frac{1}{T} \sum E_{ON} \quad (7)$$

$$P_{OFF} = \frac{1}{T} \sum E_{OFF} \quad (8)$$

$$P_{REC} = \frac{1}{T} \sum E_{REC} \quad (9)$$

The SiC Mosfet conduction loss ($P_{SiC-Mosfet_COND}$) and diode conduction loss (P_{DIODE_COND}) are calculated.

$$P_{SiC-Mosfet_COND} = \frac{1}{T} \int V_{CE} \cdot I_C \quad (10)$$

$$P_{DIODE_COND} = \frac{1}{T} \int V_F \cdot I_F \quad (11)$$

The total SiC-Mosfet losses are:

$$P_{SiC-Mosfet_TOTAL} = P_{SiC-Mosfet_COND} + P_{ON} + P_{OFF} \quad (12)$$

The total diode losses are computed in the same way as SiC-Mosfet losses, except diode turn-on losses, are considered to zero

$$P_{DIODE_TOTAL} = P_{DIODE_COND} + P_{REC} \quad (13)$$

CREE's C3M0021120K (1200 V) and C3M0025065K (650 V) devices, which are silicon carbide power MOSFETs, were applied to the converter loss analysis, respectively. In addition, for the reverse diode, Silicon Carbide Schottky Diode was applied, and CREE's C4D40120D was applied. Through this, loss analysis was performed among the operating characteristics of each converter. It derives a topology suitable for the wave power device through the efficiency analysis of each converter.

4. Comparison of Simulations and Results

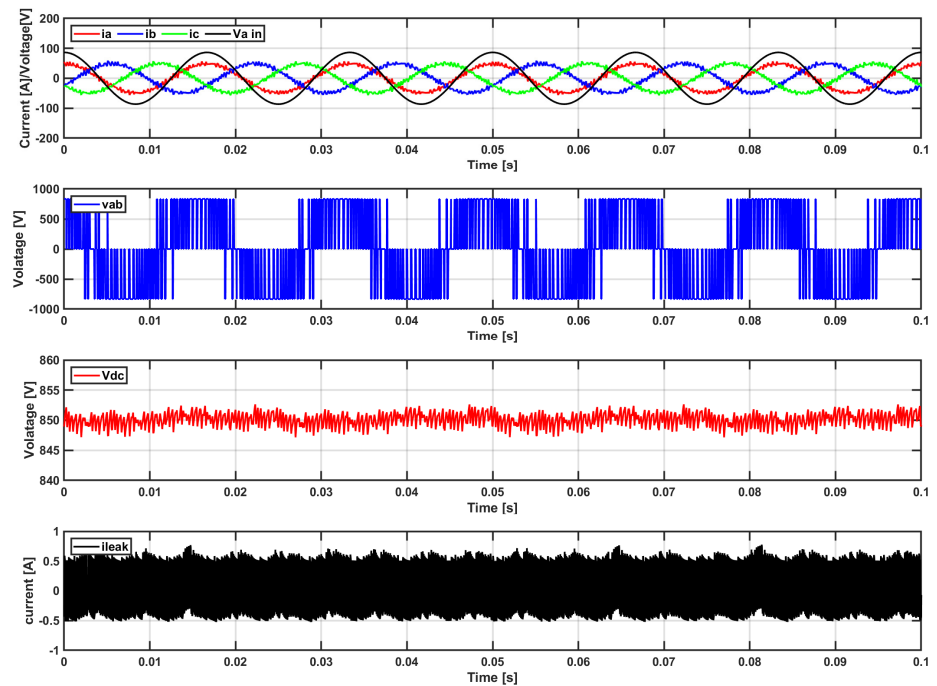
In this study, four types of topologies shown in Figure 3 were compared to select a topology suitable for wave power operating conditions. The operating conditions of the wave power generation were simulated under the rated operating conditions of 30 kW. In this study, each converter performed the operation by applying the model predictive control. The parameters of the wave power generator are shown in Table 5 below.

Table 5. Parameter for OWC-WEC Simulation.

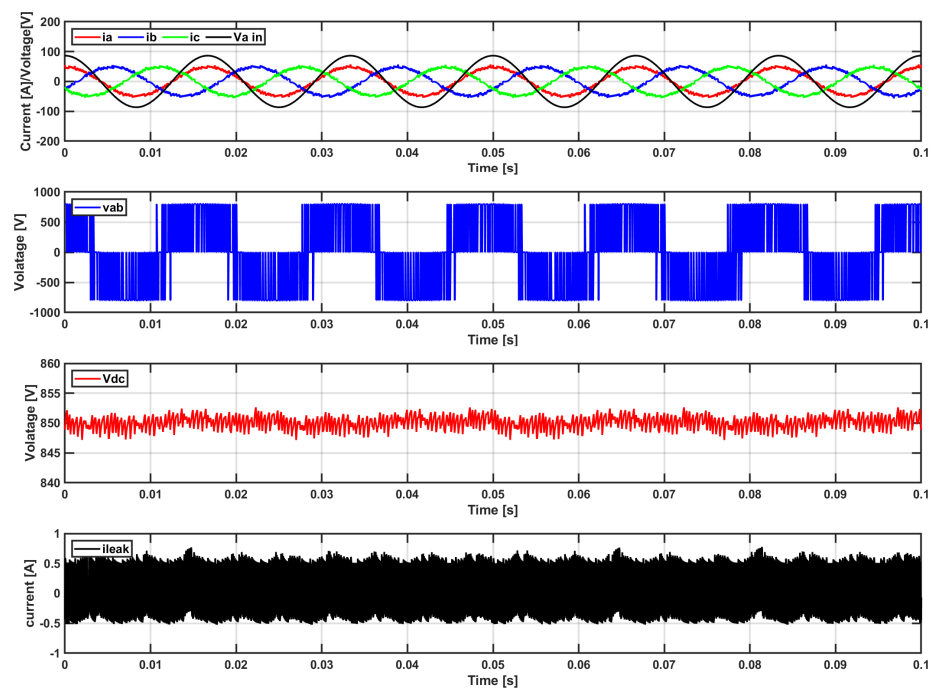
Parameters	Values
V_{in} (input voltage)	432.56 V
R_{in} (input resistance)	0.233 Ω
L_{in} (input inductance)	2.0344 mH
C_{dc} (DC capacitance)	4400 μ F
V_{dc} (DC voltage)	850 V

Figure 6 compares the output characteristics of each converter under the wave power rating conditions shown in Table 1 to confirm the performance of each converter. Model predictive control was applied to each converter. As analyzed above, it can be seen that the three-level converter is superior to the two-level converter in input current performance or input voltage performance. Also, it can be seen that the three-level converter is excellent in leakage current performance. Among them, it can be seen that the three-level four-leg converter has the best leakage current performance. In conclusion, a three-level four-

leg converter with the best input current or output performance and leakage current performance would be most suitable for a power converter for a wave power generator.



(a)



(b)

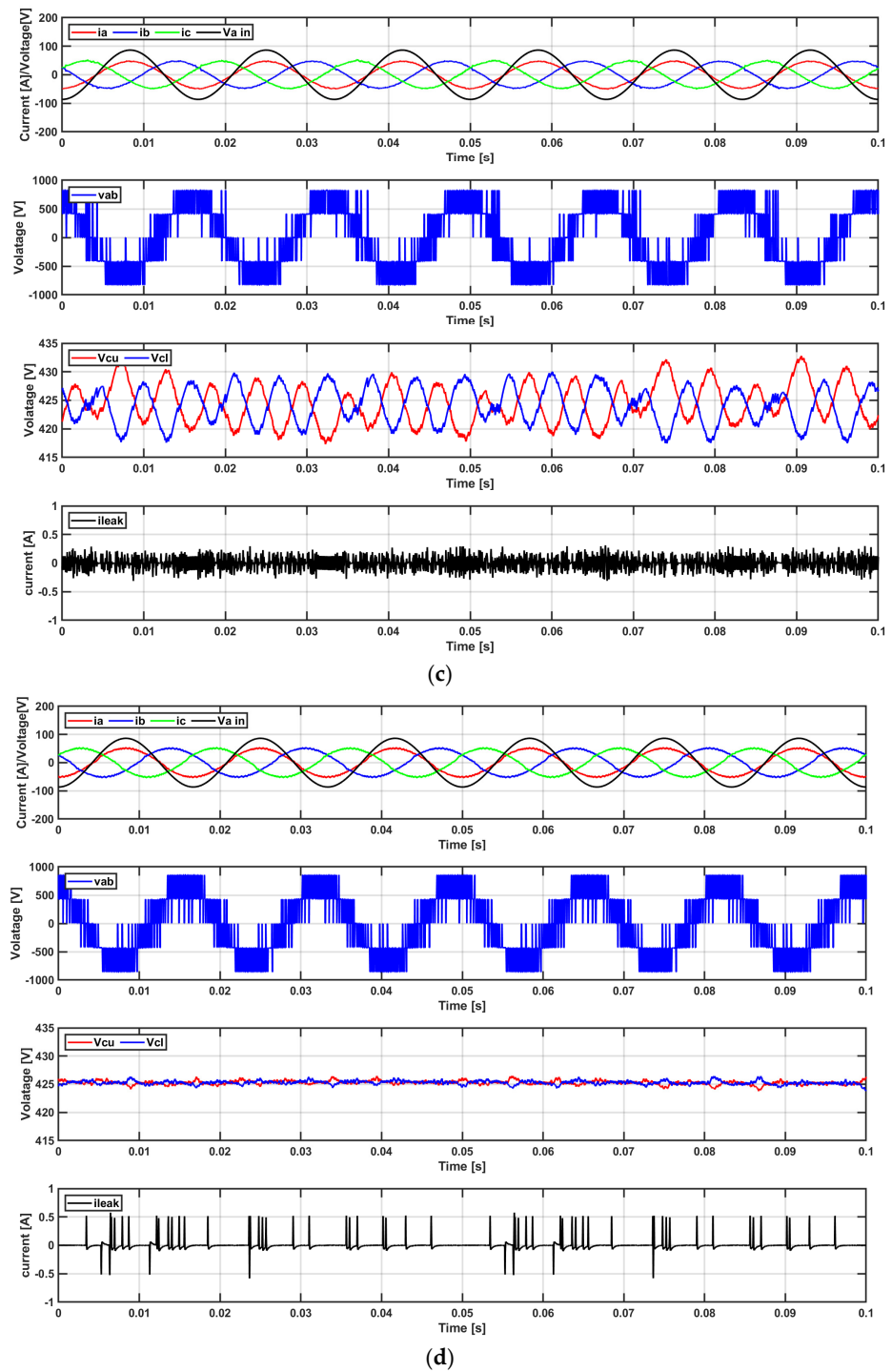


Figure 6. Comparison of output performance of four-leg converter (input current, line voltage, DC voltage, leakage current) in symmetric operation: (a) Two-level three-leg four-wire type, (b) Two-level four-leg type, (c) Three-level three-leg four-wire type, and (d) Three-level type four-leg inverter.

Figure 7 shows the dynamics of the input current for each converter. Since the wave energy of the wave power generation system changes rapidly, it must be able to follow the rapidly changing current. Model predictive control can quickly follow current changes. Figure 7 shows the current dynamics of each converter according to the reference current change. It can be seen that all converters follow the reference current quickly because model predictive control is applied, even if the input energy changes rapidly due to the nature of the wave power generation. In addition, it can be seen that the three-level converter more

accurately tracks the reference current than the two-level converter, and the current ripple is reduced, even if all converters exhibit a fast response. That is, if the model predictive control is applied to the converter for the wave power device, an advantage can be obtained.

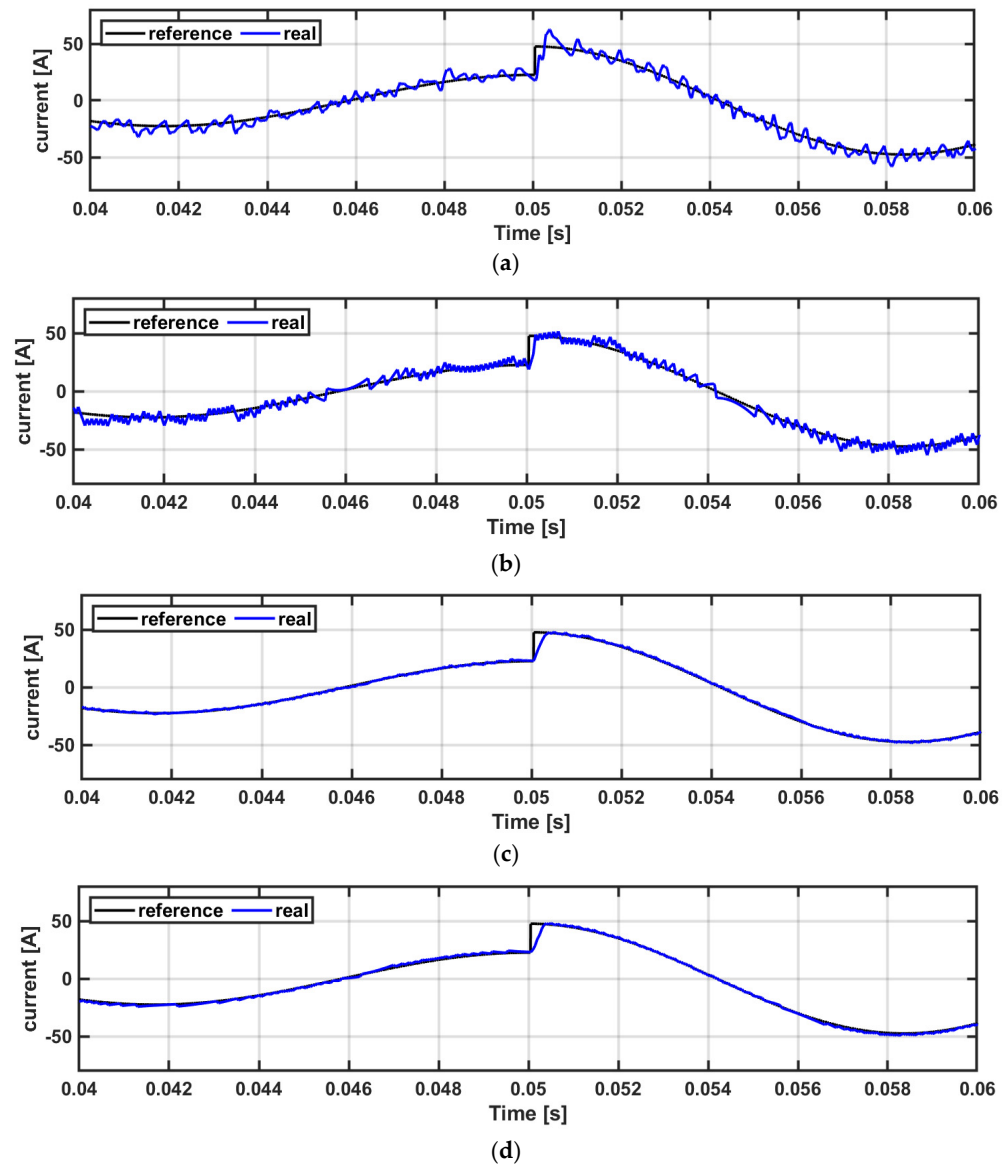


Figure 7. Comparison of output dynamics performance of four-leg converter with model predictive control: (a) two-level three-leg four-wire type, (b) two-level four-leg type, (c) three-level three-leg four-wire type and (d) three-level type four-leg inverter.

Figure 8 shows the components of the prototype for topology performance verification. Performance verification was compared by applying the two-level type and the three-level type, respectively. For the semiconductor switching element of each topology, CREE's C3M0021120K was applied for the two-level type, and CREE's C3M0025065K was applied for the three-level type. Detailed specifications of each device are shown in Table 6 below. Each topology applied the same control board, gate driver and load system, and a picture of the applied equipment is inserted in Figure 8. Through this, a performance analysis of each topology was performed. The part about signal distortion should also be considered [31]. The load parameters and operating switching frequencies for the experiment are shown in Table 7.

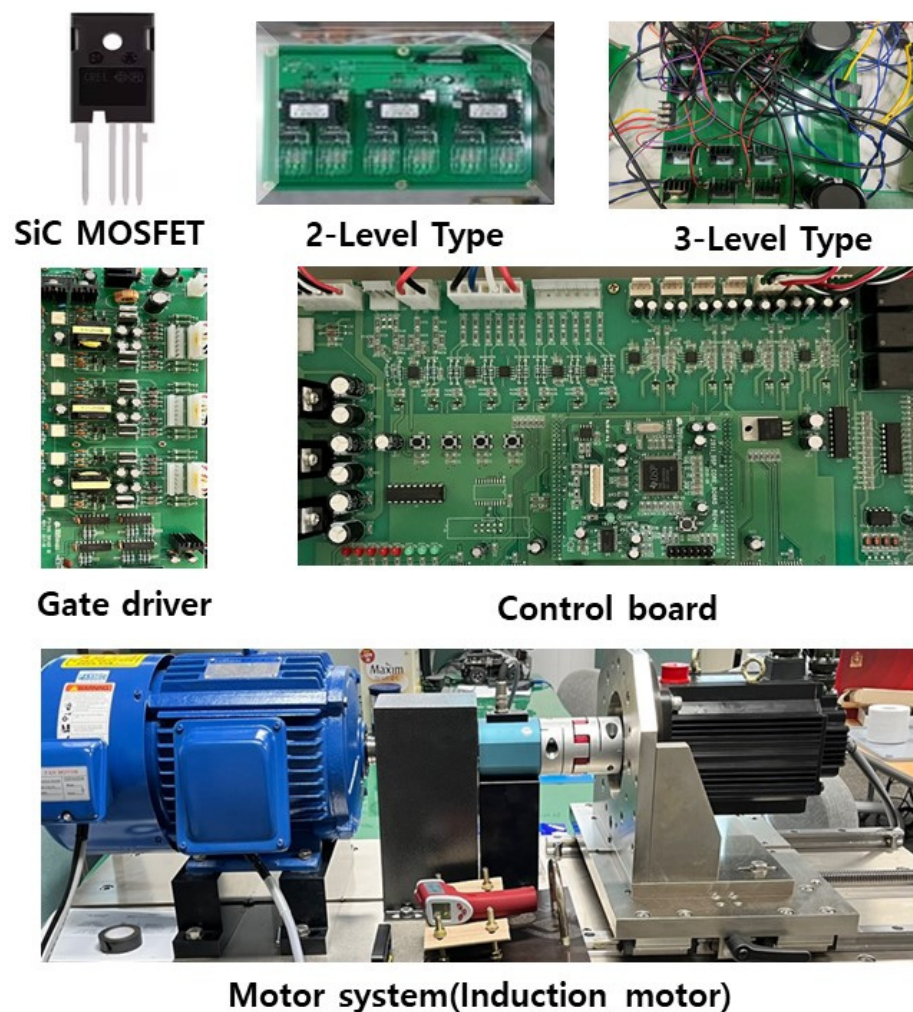


Figure 8. Pictures of prototype components for topology performance analysis.

Table 6. Semiconductor switching device specifications for topology performance verification.

	Applied Topology	V_{DS}	I_D (25 °C)	$R_{DS(ON)}$
C3M0021120K (1200 V)	Two-Level Type	1200 V	100 A	21 m Ω
C3M0025065K (650 V)	Three-Level Type	650 V	97 A	25 m Ω

Table 7. Induction Motor Parameter for inverter experiment.

Parameters	Values
R_s (stator resistance)	2 Ω
R_r (rotor resistance)	1.56 Ω
L_s (stator inductance)	54 mH
L_r (rotor inductance)	54 mH
L_m (mutual inductance)	51.5 mH
T_{sp} (sampling period)	200 μ s

Figure 9 shows the output waveform to check the operation and performance of the converter hardware. Figure 9 shows that the three-phase current and three-phase line voltage appear well in normal operation. In addition, it can be confirmed that the transient response performance is appropriately controlled by the output current size change and frequency change. Through this, it was possible to verify the corresponding algorithm through each hardware. In addition, it can be confirmed through Figure 9d that

the algorithm operates without problems, even under balanced load and unbalanced load conditions.

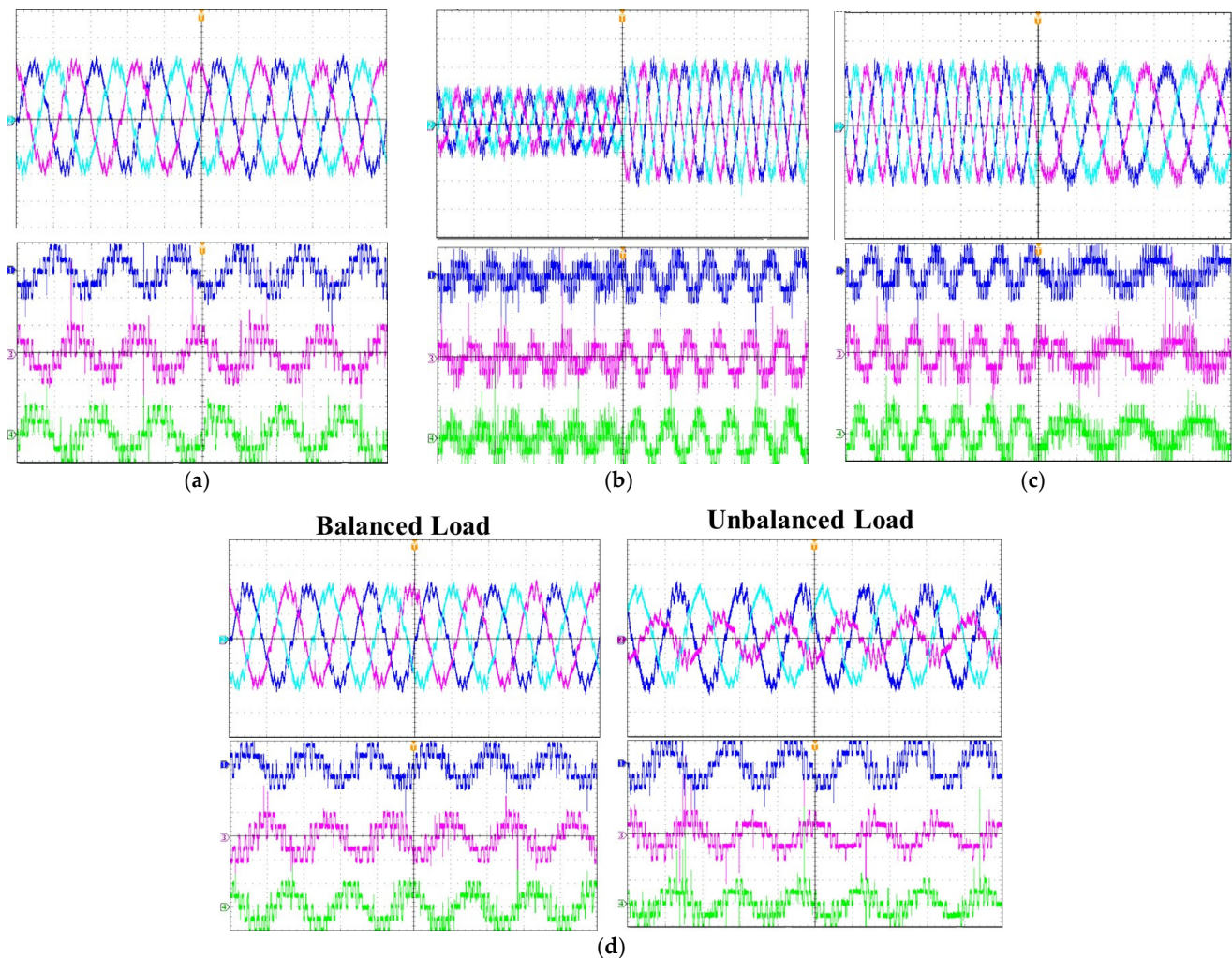


Figure 9. Output waveforms to verify converter operation: (a) steady-state operation, (b) transient response (change in output magnitude), (c) transient response (change in output frequency), (d) response to balanced and unbalanced loads.

Figure 10 shows the loss distribution of each converter element during balanced operation under rated conditions. The loss distribution is shown for each element in a-phase. For the loss analysis, the method described in Part 3 was applied. It can be seen that the three-level converter shows much less loss in each device than the two-level converter. In addition, it can be seen that the loss distribution in each device is also more balanced in the three-level converter.

Figure 11 shows the loss distribution of each converter element during unbalanced operation under rated conditions. The unbalanced operation resulted in a 1.2-fold increase in the power of a-phase. Accordingly, the overall loss increased. It was confirmed that the loss of the three-level converter was much less than that of the two-level converter in the balanced operation. Also, the loss distribution in each device was more balanced in the three-level converter. However, it can be seen that the distribution of each device is relatively constant in the three-level four-leg converter that can cope with the unbalanced operation than the three-level three-leg four-wire converter. Table 8 shows the total losses of the converter during balanced and unbalanced operations. When considered comprehensively, it can be seen that the performance of the three-level four-leg converter is the best under the wave power characteristics condition.

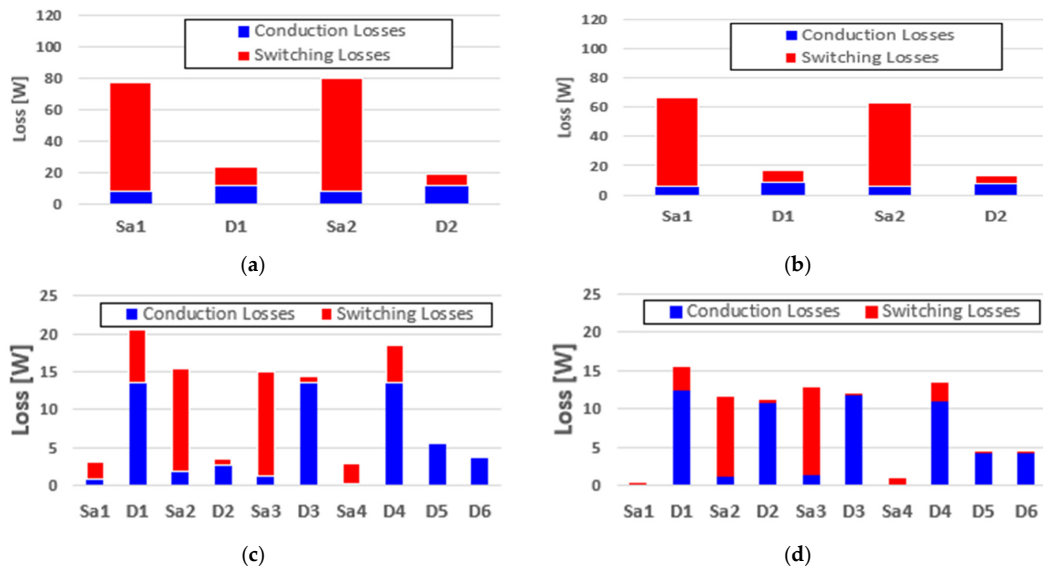


Figure 10. Comparison of power losses performance of four-leg converter (a-phase) in symmetric operation: (a) two-level three-leg four-wire type, (b) two-level four-leg type, (c) three-level three-leg four-wire type and (d) three-level type four-leg inverter.

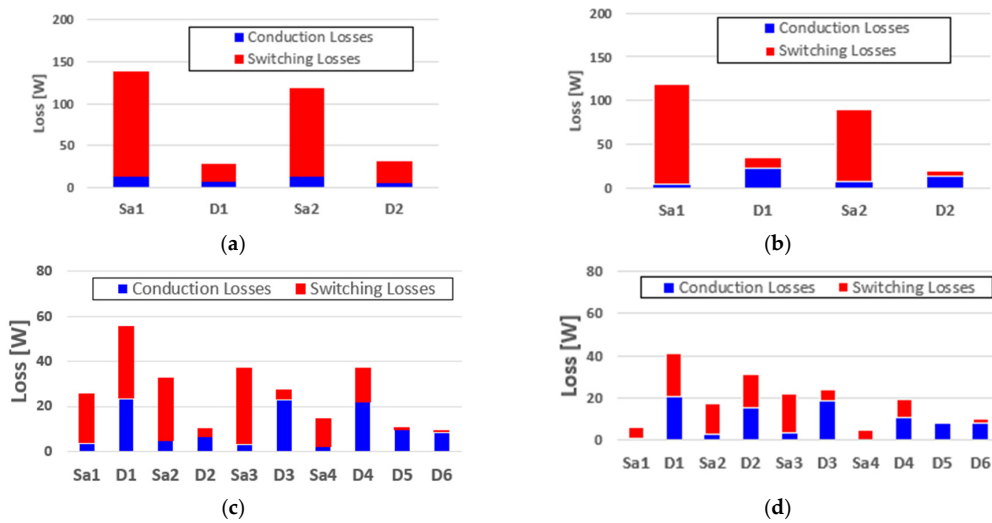


Figure 11. Comparison of power losses performance of four-leg converter (a-phase) in asymmetric operation: (a) two-level three-leg four-wire type, (b) two-level four-leg type, (c) three-level three-leg four-wire type and (d) three-level type four-leg inverter.

Table 8. Power losses under symmetric and asymmetric operation for AC/DC converter in rated operation.

		Two-Level Four-Wire	Two-Level Four-Leg	Three-Level Three-Leg Four-Wire	Three-Level Four-Leg
Losses [W]	Symmetric operation	597.75	478.89	305.79	258.26
	Asymmetric operation	899.14	752.88	693.64	490.48

Figure 12 compares the input current THD, output voltage ripple, leakage current magnitude, average switching frequency, converter loss and efficiency of each converter according to the sampling frequency change. As the sampling frequency increases, it can

be seen that the THD of the input current and the output voltage ripple decrease. The three-level, four-leg converter used in this study exhibits the lowest input current THD and low voltage ripple over all switching frequency ranges. In addition, even when the sampling frequency was changed, the three-level converter performed better than the two-level converter in terms of leakage current, and the three-level four-leg converter showed the best performance. It was also confirmed that the average switching frequency of the three-level four-leg converter was the lowest, and accordingly, it showed much superior performance than the conventional wave power converter in terms of loss and efficiency of the converter.

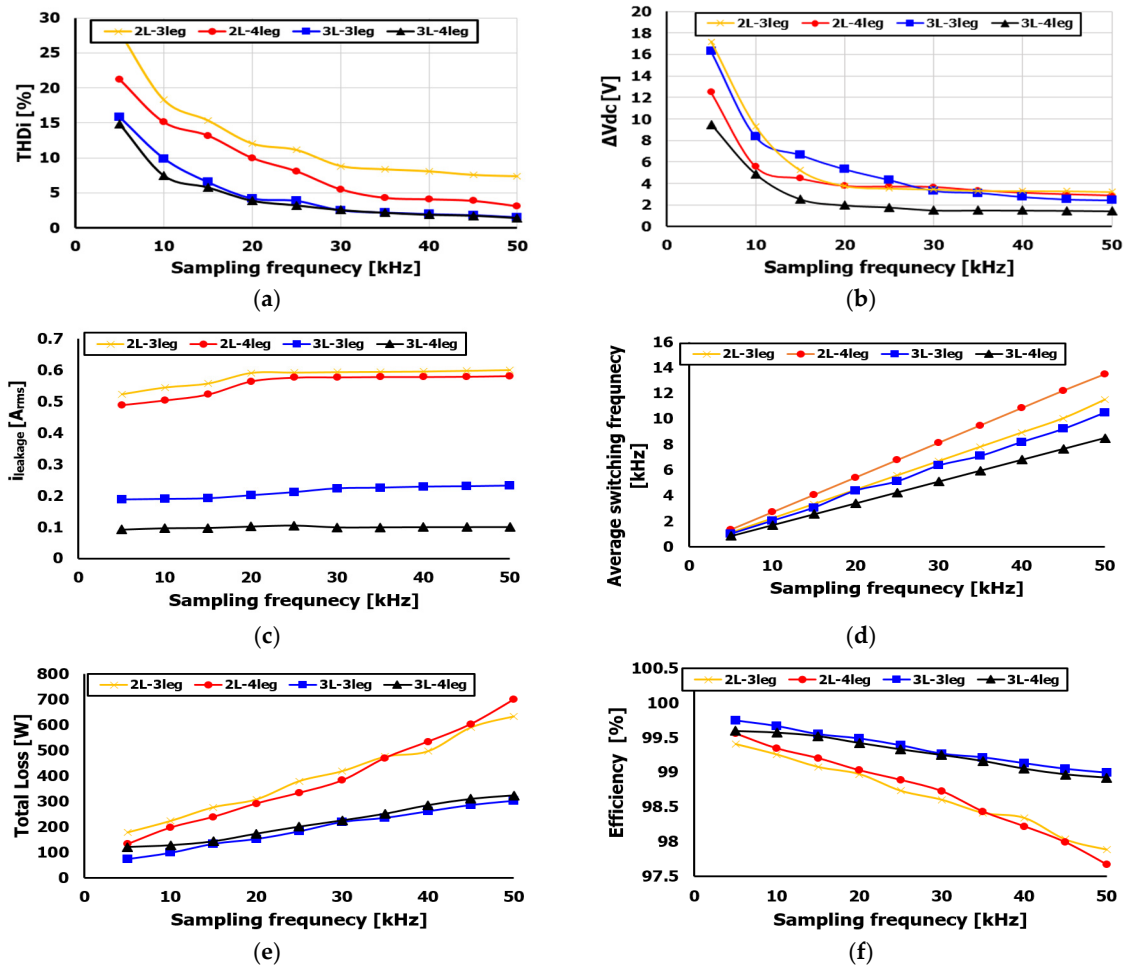


Figure 12. Comparison of output performance of four-leg converter according to sampling frequency in rated conditions: (a) THD_i , (b) capacitor voltage, (c) leakage current, (d) average switching frequency, (e) total loss and (f) efficiency.

Figure 13 compares the current THD, leakage current size, power converter loss and efficiency according to the output power change. It can be seen that the current THD and leakage current decrease as the output power increases, similar to the characteristics according to the sampling frequency change. In addition, it can be seen that loss and efficiency also improve as the output power increases. Depending on the output power change, the three-level converter showed better performance than the two-level converter, and the three-level four-leg converter showed the best performance.

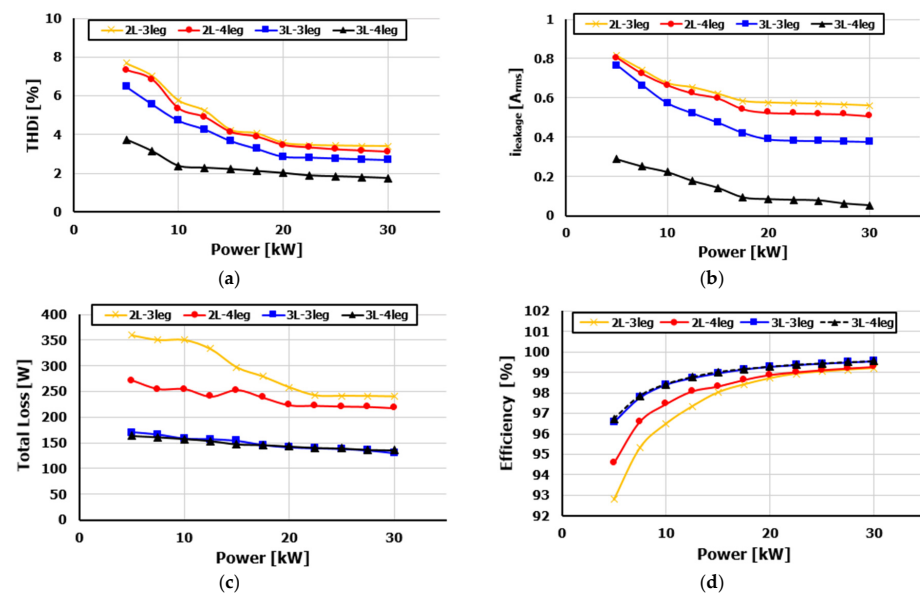


Figure 13. Comparison of output performance of four-leg converter according to output power: (a) THD_i, (b) leakage current, (c) total loss, and (d) efficiency.

Figure 14 shows the distribution of losses of each inverter element under a balanced load under rated conditions. The loss distribution is shown for each element in a-phase. As in the converter analysis, it can be seen that the three-level converter shows much less loss in each device than the two-level converter. In addition, Figure 15 shows the distribution of losses of each inverter element during unbalanced operation under rated conditions. The unbalanced operation increased the overall loss because the a-phase power increased by a factor of 1.2. It was confirmed that the loss of the three-level converter was much less than that of the two-level converter in the balanced operation. Similar to the converter analysis, the three-level inverter shows lower losses than the two-level inverter. The maximum efficiency difference was 2.28% higher for the three-level four-leg converter in balanced operation and 2.7% higher in unbalanced operation. Table 9 shows the efficiency of the power converter for wave power generation incorporating the converter-inverter during balanced and unbalanced operations.

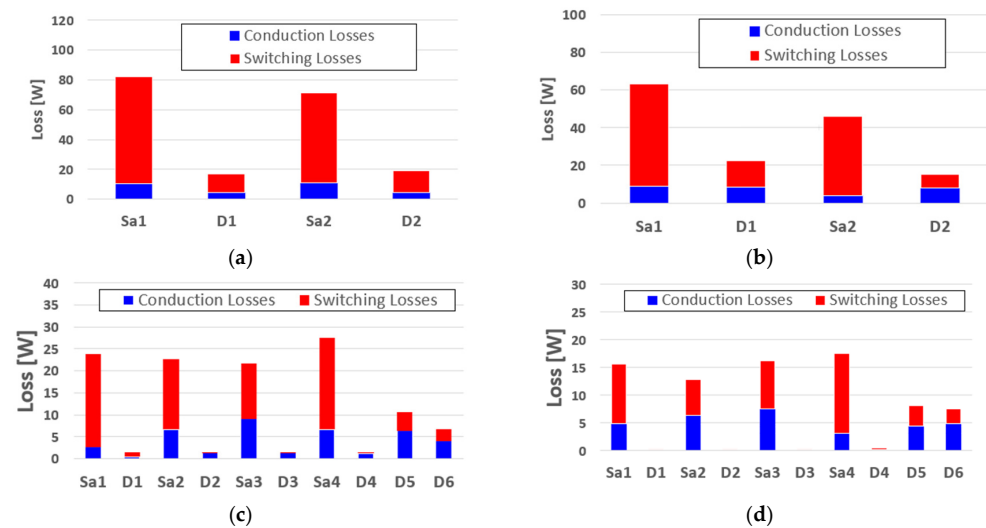


Figure 14. Comparison of power losses performance of four-leg inverter (a-phase) in symmetric operation: (a) Two-level three-leg four-wire type, (b) Two-level four-leg type, (c) Three-level three-leg four-wire type, and (d) Three-level type four-leg inverter.

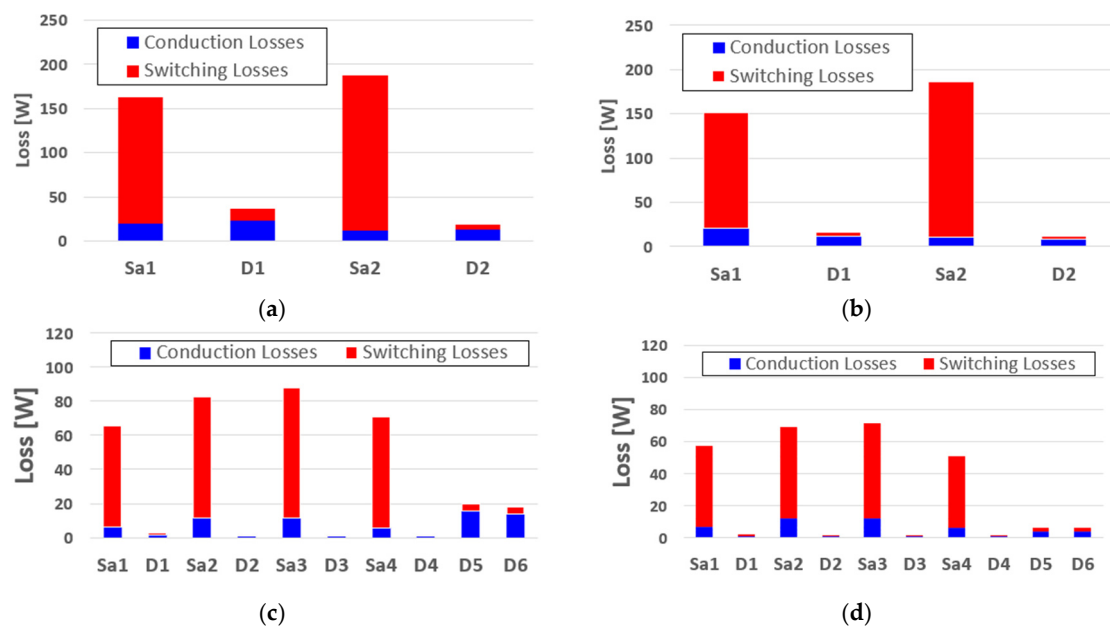


Figure 15. Comparison of power losses performance of four-leg inverter (a-phase) in asymmetric operation: (a) Two-level three-leg four-wire type, (b) Two-level four-leg type, (c) Three-level three-leg four-wire type, and (d) Three-level type four-leg inverter.

Table 9. Total Efficiency under symmetric and asymmetric operation for DC/AC inverter in rated operation.

		Two-Level Three-Leg Four-Wire	Two-Level Four-Leg	Three-Level Three-Leg Four-Wire	Three-Level Four-Leg
Total Efficiency [%]	Symmetric operation	96.0	96.8	97.96	98.28
	Asymmetric operation	94.0	95.0	95.4	96.7

5. Conclusions

In order to increase the energy efficiency of the wave power generator, it is essential to increase the efficiency of the power converter. Efficient converters must operate at low switching frequencies, which increases the weight and volume of passive components, which can exceed space constraints. Therefore, in this paper, we compare the performance of various types of topologies, from the two-level topology to the three-level topology applied to the existing wave power generation device. In particular, analysis was performed focusing on a four-leg type topology that can cope with unbalanced operation, and model predictive control was applied to apply to abrupt energy changes and atypical topologies. As a power converter for wave power generation, a three-level, four-leg topology with the best current harmonics, leakage current performance, DC voltage fluctuation rate and loss is suitable. This was the best performance of the three-level four-leg topology, even with the switching frequency change affecting the topology performance. The three-level four-leg back-to-back converter showed up to 2.28% and 2.7% higher efficiencies under balanced and unbalanced operating conditions. In conclusion, a three-level, four-leg topology is most suitable as a power converter for wave power generation under the same conditions.

Funding: This research was supported by Basic Science Research Program through the National Research Foundation of Korea(NRF) funded by the Ministry of Education(No. RS-2022-00165789).

Conflicts of Interest: The author declares no conflict of interest.

References

1. Lopéz, I.; Andreu, J.; Ceballos, S.; de Alegría, I.M.; Kortabarria, I. Review of wave energy technologies and the necessary power-equipment. *Renew. Sustain. Energy Rev.* **2013**, *27*, 413–434. [[CrossRef](#)]
2. Reguero, B.; Losada, I.; Méndez, F. A global wave power resource and its seasonal, interannual and long-term variability. *Appl. Energy* **2015**, *148*, 366–380. [[CrossRef](#)]
3. Taveira-Pinto, F.; Rosa-Santos, P.; Fazeres-Ferradosa, T. Marine renewable energy. *Renew. Energy* **2020**, *150*, 1160–1164. [[CrossRef](#)]
4. Kalogeri, C.; Galanis, G.; Spyrou, C.; Diamantis, D.; Baladima, F.; Koukoula, M.; Kallos, G. Assessing the European offshore wind and wave energy resource for combined exploitation. *Renew. Energy* **2017**, *101*, 244–264. [[CrossRef](#)]
5. Fusco, F.; Nolan, G.; Ringwood, J.V. Variability reduction through optimal combination of wind/wave resources—An Irish case study. *Energy* **2010**, *35*, 314–325. [[CrossRef](#)]
6. Reikard, G.; Robertson, B.; Bidlot, J.-R. Combining wave energy with wind and solar: Short-term forecasting. *Renew. Energy* **2015**, *81*, 442–456. [[CrossRef](#)]
7. Schweizer, M.; Lizama, I.; Friedli, T.; Kolar, J.W. Comparison of the chip area usage of 2-level and 3-level voltage source converter topologies. In Proceedings of the IECON 2010—36th Annual Conference on IEEE Industrial Electronics Society, Glendale, AZ, USA, 7–10 November 2010; pp. 391–396.
8. Teichmann, R.; Bernet, S. A comparison of three-level converters versus two-level converters for low-voltage drives, traction, and utility applications. *IEEE Trans. Ind. Appl.* **2005**, *41*, 855–865. [[CrossRef](#)]
9. Schweizer, M.; Friedli, T.; Kolar, J.W. Comparative evaluation of advanced three-phase three-level inverter/converter topologies against two-level systems. *IEEE Trans. Ind. Electron.* **2012**, *60*, 5515–5527. [[CrossRef](#)]
10. Moreira, A.; Lipo, T.; Venkataramanan, G.; Bernet, S. High-frequency modeling for cable and induction motor overvoltage studies in long cable drives. *IEEE Trans. Ind. Appl.* **2002**, *38*, 1297–1306. [[CrossRef](#)]
11. JStröm, P.; Korhonen, J.; Tyster, J.; Silventoinen, P. Active du/dt—New output-filtering approach for inverter-fed electric drives. *IEEE Trans. Ind. Electron.* **2011**, *58*, 3840–3847. [[CrossRef](#)]
12. Bendjedja, M.; Tehrani, K.A.; Azzouz, Y. Design of RST and fractional order PID controllers for an induction motor drive for electric vehicle application. In Proceedings of the 7th IET International Conference on Power Electronics, Machines and Drives (PEMD 2014), Manchester, UK, 8–10 April 2014.
13. Poblete, P.; Pereda, J.; Nuñez, F.; Aguilera, R.P. Distributed current control of cascaded multilevel inverters. In Proceedings of the 2019 IEEE International Conference on Industrial Technology (ICIT), Melbourne, VIC, Australia, 13–15 February 2019; pp. 1509–1514.
14. Chaturvedi, P.; Jain, S.; Agarwal, P. Carrier-based common mode voltage control techniques in three-level diode-clamped inverter. *Adv. Power Electron.* **2012**, *2012*, 327157. [[CrossRef](#)]
15. Videt, A.; Le Moigne, P.; Idir, N.; Baudesson, P.; Cimetiere, X. A new carrier-based PWM providing common-mode-current reduction and DC-bus balancing for three-level inverters. *IEEE Trans. Ind. Electron.* **2007**, *54*, 3001–3011. [[CrossRef](#)]
16. Djeghloud, H.; Benalla, H. Space vector pulse width modulation applied to the three-level voltage inverter. *IEEE Trans. Power Electron.* **2004**, *19*, 732–738.
17. Busquets-Monge, S.; Bordonau, J.; Boroyevich, D.; Somavilla, S. The nearest three virtual space vector PWM—a modulation for the comprehensive neutral-point balancing in the three-level NPC inverter. *IEEE Power Electron. Lett.* **2004**, *2*, 11–15. [[CrossRef](#)]
18. Mohapatra, S.R.; Agarwal, V. Model predictive controller with reduced complexity for grid-tied multilevel inverters. *IEEE Trans. Ind. Electron.* **2018**, *66*, 8851–8855. [[CrossRef](#)]
19. Yamasu, V.; Rivera, M.; Wu, B.; Rodriguez, J. Model predictive current control of two-level four-leg inverters—Part I: Concept, algorithm, and simulation analysis. *IEEE Trans. Power Electron.* **2012**, *28*, 3459–3468. [[CrossRef](#)]
20. Kim, S.E.; Park, S.Y.; Kwak, S. Simplified model predictive control method for three-phase four-leg voltage source inverters. *J. Power Electron.* **2016**, *16*, 2231–2242. [[CrossRef](#)]
21. Roh, C.; Kim, K.H.; Park, J.Y.; Kwak, S.S. Simplified model predictive control with preselection technique for reduction of calculation burden in 3-level 4-leg NPC inverter. In Proceedings of the 2020 IEEE Applied Power Electronics Conference and Exposition (APEC), New Orleans, LA, USA, 15–19 March 2020; pp. 2291–2296.
22. Roh, C.; Kwak, S.; Choi, S. Three-phase three-level four-leg NPC converters with advanced model predictive control. *J. Power Electron.* **2021**, *21*, 1574–1584. [[CrossRef](#)]
23. Mohapatra, S.R.; Agarwal, V. An improved reduced complexity model predictive current controller for grid-connected four-leg multilevel inverter. *IEEE Trans. Ind. Appl.* **2019**, *56*, 498–506. [[CrossRef](#)]
24. Nabae, A.; Takahashi, I.; Akagi, H. A new neutral-point-clamped PWM inverter. *IEEE Trans. Ind. Appl.* **1981**, *IA-17*, 518–523. [[CrossRef](#)]
25. Poorfakhraei, A.; Narimani, M.; Emadi, A. A review of multilevel inverter topologies in electric vehicles: Current status and future trends. *IEEE Open J. Power Electron.* **2021**, *2*, 155–170. [[CrossRef](#)]
26. Nazer, A.; Driss, S.; Haddadi, A.M.; Farhangi, S. Optimal photovoltaic multi-string inverter topology selection based on reliability and cost analysis. *IEEE Trans. Sustain. Energy* **2020**, *12*, 1186–1195. [[CrossRef](#)]
27. Kim, J.C.; Kim, D.; Kwak, S.S. Direct Power-Based Three-Phase Matrix Rectifier Control with Input Power Factor Adjustment. *Electronics* **2019**, *8*, 1427. [[CrossRef](#)]

28. Kwak, S.; Park, J.C. Predictive control method with future zero-sequence voltage to reduce switching losses in three-phase voltage source inverters. *IEEE Trans. Power Electron.* **2014**, *30*, 1558–1566. [[CrossRef](#)]
29. Roh, C. Performance Comparisons of Three-Phase/Four-Wire Model Predictive Control-Based DC/AC Inverters Capable of Asymmetric Operation for Wave Energy Converters. *Energies* **2022**, *15*, 2839. [[CrossRef](#)]
30. Blaabjerg, F.; Jaeger, U.; Munk-Nielsen, S. Power losses in PWM-VSI inverter using NPT or PT IGBT devices. *IEEE Trans. Power Electron.* **1995**, *10*, 358–367. [[CrossRef](#)]
31. Havlík, M.; Libra, M.; Poulek, V.; Kouřim, P. Analysis of Output Signal Distortion of Galvanic Isolation Circuits for Monitoring the Mains Voltage Waveform. *Sensors* **2022**, *22*, 7769. [[CrossRef](#)]

Disclaimer/Publisher’s Note: The statements, opinions and data contained in all publications are solely those of the individual author(s) and contributor(s) and not of MDPI and/or the editor(s). MDPI and/or the editor(s) disclaim responsibility for any injury to people or property resulting from any ideas, methods, instructions or products referred to in the content.